

Combating multidrug-resistant Gram-negative bacteria with structurally nanoengineered antimicrobial peptide polymers

Shu J. Lam¹, Neil M. O'Brien-Simpson², Namfon Pantarat², Adrian Sulistio¹, Edgar H. H. Wong¹, Yu-Yen Chen², Jason C. Lenzo², James A. Holden², Anton Blencowe^{1,3}, Eric C. Reynolds^{2*} and Greg G. Qiao^{1*}

With the recent emergence of reports on resistant Gram-negative 'superbugs', infections caused by multidrug-resistant (MDR) Gram-negative bacteria have been named as one of the most urgent global health threats due to the lack of effective and biocompatible drugs. Here, we show that a class of antimicrobial agents, termed 'structurally nanoengineered antimicrobial peptide polymers' (SNAPPs) exhibit sub- μ M activity against all Gram-negative bacteria tested, including ESKAPE and colistin-resistant and MDR (CMDR) pathogens, while demonstrating low toxicity. SNAPPs are highly effective in combating CMDR *Acinetobacter baumannii* infections *in vivo*, the first example of a synthetic antimicrobial polymer with CMDR Gram-negative pathogen efficacy. Furthermore, we did not observe any resistance acquisition by *A. baumannii* (including the CMDR strain) to SNAPPs. Comprehensive analyses using a range of microscopy and (bio) assay techniques revealed that the antimicrobial activity of SNAPPs proceeds via a multimodal mechanism of bacterial cell death by outer membrane destabilization, unregulated ion movement across the cytoplasmic membrane and induction of the apoptotic-like death pathway, possibly accounting for why we did not observe resistance to SNAPPs in CMDR bacteria. Overall, SNAPPs show great promise as low-cost and effective antimicrobial agents and may represent a weapon in combating the growing threat of MDR Gram-negative bacteria.

A group of pathogens responsible for the majority of hospital-acquired infections—commonly referred to as the 'ESKAPE' pathogens—have been named as one of the biggest threats to health as a result of their multidrug resistance^{1–3}. Although the Gram-positive bacteria in the ESKAPE group, including the methicillin-resistant *Staphylococcus aureus*, have rightly drawn attention over the past decade, infections caused by the Gram-negative microbes have recently been recognized as a more critical healthcare issue^{4,5}. Despite the fact that many Gram-negative bacteria have acquired antibiotic resistance, the pipeline for the development of new antimicrobials that target Gram-negative bacteria remains empty⁶. The dearth of drug candidates against Gram-negative bacteria is attributed to the fact that they might be harder to kill than Gram-positive bacteria, largely due to the presence of an outer membrane (OM) that serves as a highly impermeable barrier, as well as additional defence mechanisms that might be absent in Gram-positive bacteria^{4,7}.

Antimicrobial peptides (AMPs) have been widely regarded as a promising solution to combat MDR bacteria⁸. Unlike conventional antibiotics, which act on specific intracellular targets⁹, AMPs interact with microbial membranes through electrostatic interactions and physically damage the bacterial morphology¹⁰. The nature of this antimicrobial mechanism renders bacteria less likely to develop resistance to AMPs. However, AMPs have had limited success in clinical settings (with the exception of a few promising candidates being evaluated as topical agents, such as omiganan¹¹), primarily due to their high toxicity towards mammalian cells¹². Recently, ring-opening polymerization

(ROP) of α -amino acid *N*-carboxyanhydrides (NCAs) has been shown to be a versatile method for the synthesis of peptide polymers with antimicrobial properties^{13,14}, even though NCA-ROP cannot rival the precise peptide sequences obtained via solid-phase peptide synthesis. Nevertheless, advances in NCA-ROP have provided a facile route for the synthesis of well-defined peptide polymers with complex macromolecular architectures, such as star polymer nanoparticles^{15,16}. We, along with several other research groups, have recently reported studies that demonstrated the potential of these star-shaped peptide polymer nanoparticles in nanomedicine¹⁷, particularly in the fields of gene therapy^{18,19} and targeted drug delivery²⁰.

In this study, we report the discovery of star-shaped peptide polymer nanoparticles consisting of lysine and valine residues, synthesized via NCA-ROP, as a new class of antimicrobial agents. These star nanoparticles were termed 'structurally nanoengineered antimicrobial peptide polymers' (SNAPPs). Unlike existing self-assembled antimicrobial macromolecules, which will dissociate to unimers below their critical micelle concentration^{21,22}, SNAPPs are stable unimolecular architectures up to infinite dilution. We demonstrate that SNAPPs exhibit superior antibacterial activity against a range of clinically important Gram-negative bacteria, possess high therapeutic indices and display selectivity towards pathogens over mammalian cells. Crucially, we show that SNAPPs can combat CMDR *A. baumannii* infection in mice. We also show that SNAPPs have a multimodal antimicrobial mechanism involving disruption of the integrity of the OM, cytoplasmic membrane (CM) disruption, unregulated ion efflux/influx and induction

¹Polymer Science Group, Department of Chemical & Biomolecular Engineering, The University of Melbourne, Parkville, Victoria 3010, Australia. ²Melbourne Dental School and The Bio21 Institute of Molecular Science and Biotechnology, Oral Health CRC, The University of Melbourne, Parkville, Victoria 3010, Australia. ³School of Pharmacy and Medical Sciences, Division of Health Sciences, The University of South Australia, Adelaide, South Australia 5000, Australia. *e-mail: e.reynolds@unimelb.edu.au; gregghq@unimelb.edu.au

Table 1 | Antimicrobial activity of SNAPPs and other peptides against a range of Gram-negative pathogens.

Antimicrobial type	Code/name	Medium	MBC* (μ M)					
			<i>E. coli</i>	<i>P. aeruginosa</i>	<i>K. pneumoniae</i>	<i>A. baumannii</i>	CMDR <i>P. aeruginosa</i>	CMDR <i>A. baumannii</i>
SNAPP	S16	MHB	0.72 ± 0.06	1.42 ± 0.08	1.54 ± 0.08	0.85 ± 0.05	1.38 ± 0.03	1.61 ± 0.23
		MEM	0.17 ± 0.01	0.07 ± 0.04	0.19 ± 0.05	0.05 [†]	0.08 [†]	0.05 ± 0.01
	S32	MHB	0.72 ± 0.54	0.97 ± 0.05	0.83 ± 0.14	0.79 ± 0.02	1.00 [†]	0.85 ± 0.03
		MEM	0.05 ± 0.01	0.02 [†]	0.08 ± 0.02	0.02 [†]	0.03 ± 0.01	0.03 ± 0.01
AMP	Ovispirin [‡]	MHB	8.39 ± 0.44	95.49 ± 9.73	11.49 ± 4.86	2.21 ± 0.88	Not tested	Not tested
	Magainin II [‡]	MHB	47.85 ± 6.08	55.96 ± 2.84	154.59 ± 9.32	19.87 ± 3.24	Not tested	Not tested
	Melittin [‡]	MHB	33.71 ± 5.18	29.37 ± 8.24	109.25 ± 20.43	0.91 ± 0.09	Not tested	Not tested

*MBC is defined as the minimum drug concentration that causes quantitative bacterial cell death (see Methods, Supplementary Fig. 9 and Supplementary Table 2 for further clarification). All data are expressed as mean and s.d. of four replicates ($n=4$) completed in two independent experiments; [†]MBC values were identical across all replicates; [‡]The amino acid sequences of ovispirin, magainin II and melittin are KNLRIIRKIIHIKKYD-COOH, GIGKFLHSACKFGKAFCVGEIMNS-CONH₂ and GIGAVILKVLTGALPALSWKRKRRQQ-COOH, respectively. Ovispirin, magainin II and melittin were synthesized using standard solid-phase peptide synthesis protocols for Fmoc (9-fluorenylmethoxy carbonyl) chemistry (see Methods for details) and their antimicrobial activities were evaluated as per SNAPPs.

of apoptotic-like death (ALD), which potentially accounts for the superior performance of SNAPPs and differs from that typically reported for most AMPs.

Results and discussion

Synthesis and characterization of SNAPPs. To demonstrate the potential of this new class of antimicrobial nanomaterial, SNAPPs in the form of 16- and 32-arm star peptide polymer nanoparticles **S16** and **S32**, respectively, were synthesized via NCA-ROP (number-average molecular weight, $M_n = 43.8$ kDa (**S16**), 74.8 kDa (**S32**); hydrodynamic diameter, $D_H = 7.7$ nm (**S16**), 13.5 nm (**S32**); Fig. 1, Supplementary Section ‘Synthesis and Characterization of SNAPPs’, Supplementary Figs 1–8 and Supplementary Table 1), in a similar fashion to that reported by us¹⁸. Inspired by naturally occurring AMPs where the mode of action has been partly attributed to a positively charged amphipathic structure⁸ and after taking into account various synthetic considerations, lysine and valine were selected as cationic and hydrophobic amino acids, respectively. Their monomeric NCA derivatives were randomly polymerized from a PAMAM dendritic core to form the star arms with a theoretical lysine-to-valine ratio of 2:1, which was selected to promote water solubility and an average degree of polymerization (DP) of 30 residues per star arm at complete monomer conversion.

In vitro antimicrobial properties of SNAPPs. We evaluated the antibacterial efficacy of SNAPPs by determining their minimum bactericidal concentrations (MBCs) against a range of Gram-positive (*Streptococcus mutans* and *S. aureus*) and Gram-negative (*Escherichia coli*, *Pseudomonas aeruginosa*, *Klebsiella pneumoniae* and *A. baumannii*) bacteria. The MBC is defined as the minimum drug concentration that causes quantitative cell death (see Methods, Supplementary Fig. 9 and Supplementary Table 2 for further clarification). The antimicrobial susceptibility assays were initially conducted in Mueller–Hinton broth (MHB), a nutrient-rich bacterial growth medium. Our initial studies, which focused on the two Gram-positive bacteria (*S. aureus* and *S. mutans*) and two Gram negative bacteria (*E. coli* and *P. aeruginosa*) showed that **S16** and **S32** had preferential activity towards the Gram-negative species (MBC < 1.4 μ M; Table 1) over the Gram-positive strains (MBC > 1.8 μ M) (Supplementary Table 3). It is worth noting that homolysine star-shaped peptide polymer nanoparticles, that is, those that do not contain valine residues, exhibited a higher MBC value (greater than threefold increase in MBC against *E. coli*), thus demonstrating the need for an amphipathic structure to effect antimicrobial activity.

In further studies using Gram-negative bacteria, **S16** and **S32** were also found to be effective against *K. pneumoniae* and *A. baumannii*, with **S16** registering MBC values of 1.54 and 0.85 μ M, respectively, and **S32** showing similar MBC values of 0.83 and 0.79 μ M.

Furthermore, both **S16** and **S32** were found to be equally effective against CMDR clinical isolates of *P. aeruginosa* (FADDI-PA067) and *A. baumannii* (FADDI-AB156) (Supplementary Tables 4 and 5) as to drug-sensitive strains, yielding MBC values ranging from 0.85 to 1.61 μ M (Table 1). We observed that the MBC values of SNAPPs against all bacteria tested were within a similar order of magnitude, which implied that the antimicrobial efficacies of **S16** and **S32** might not be species-specific for Gram-negative bacteria. This was surprising, as *P. aeruginosa* and *K. pneumoniae* possess low antibiotic susceptibility as a result of their thick extracellular capsules, which contribute to reduced cell permeability²³ and are a resistance mechanism against antibiotics and AMPs^{24,25}. It is noteworthy that the probability of the PAMAM dendrimer cores contributing to the antimicrobial efficacies of **S16** and **S32** in this study was discounted, as the PAMAM cores were found to be non-active against the range of bacterial species tested above (Supplementary Table 6).

We also conducted an antimicrobial resistance study to evaluate if resistance against SNAPPs could be generated easily. Following serial passaging of bacterial cells in the presence of sub-MBC levels of **S16**, we did not obtain *de novo* resistant mutants of wild-type and CMDR *A. baumannii* to **S16**, even after 600 generations of growth (over a period of 24 days) (Supplementary Fig. 10). The MBC values of **S16** against these bacterial strains remained relatively constant throughout the experiment, despite the fact that the CMDR strain is genetically capable of mutation and rapid resistance acquisition. This result suggests that resistance to SNAPPs is not acquired easily.

As a comparator, we synthesized the linear analogue **L** to represent one arm of **S16** and **S32** (Supplementary Figs 11–13 and Supplementary Table 7). Interestingly, compared to SNAPPs, the linear analogue was poorly active against *E. coli* and *S. aureus*, with MBCs at least 40-fold higher than those of SNAPPs (Supplementary Table 8). We hypothesize that the star architecture has a significant effect on enhancing the antimicrobial action of random co-peptide polymers against bacteria. Similar to that observed by Yang and co-workers, we theorize that the improvement in activity is a result of the increased local concentration of charges provided by the nanostructure, thereby leading to greater ionic interactions with the bacterial membranes²². Additionally, bacterial membrane-induced peptide aggregation has been postulated to be a key factor of AMP efficacy, as it enables AMPs to achieve the high threshold concentrations needed for membrane disruption²⁶. Extending this concept, we hypothesize that the star architecture affords a high local concentration of peptide mass, even in solution, before contacting bacterial cells, which may contribute to the enhanced efficacy of SNAPPs.

The antimicrobial activities of **S16** and **S32** were compared with several peptide-based antimicrobial agents known to be effective

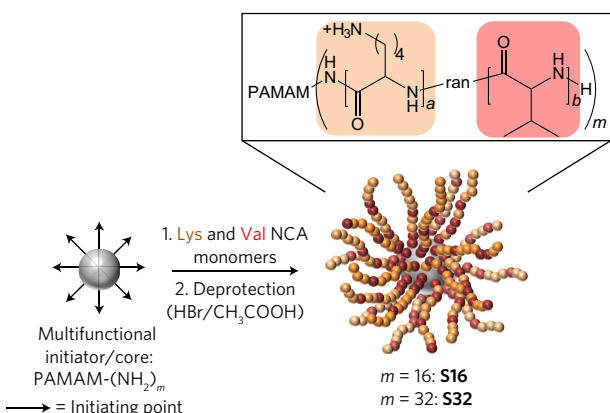


Figure 1 | Synthesis of SNAPPs. Synthesis of SNAPPs via ring-opening polymerization of lysine and valine *N*-carboxyanhydrides (NCAs) was initiated from the terminal amines of poly(amido amine) (PAMAM) dendrimers. Second- and third-generation PAMAM dendrimers (see Supplementary Fig. 2 for the structure of the former) with 16 and 32 peripheral primary amines were used to prepare 16- and 32-arm SNAPPs, respectively. Note that the number of initiating points on the figure does not reflect the actual number, which is 16 or 32. The number of repeat units for lysine and valine are *a* and *b*, respectively. The lysine-to-valine ratios (*a:b*) are provided in Supplementary Table 1.

against Gram-negative pathogens, including magainin II, ovispirin and melittin (Table 1). The antimicrobial efficacies of these AMPs against certain Gram-negative pathogens have been well-documented; however, they (as is the case with most AMPs) tend to demonstrate selective activity towards certain bacterial strains, even within the Gram-negative family (Table 1). This is in direct contrast to SNAPPs which displayed effective equipotent activity against all of the Gram-negative species tested. Furthermore, SNAPPs were orders of magnitude more effective than these AMPs (Table 1).

To explore the antimicrobial efficacy of SNAPPs in different media and to evaluate their toxicity against mammalian cells, we repeated the assays using minimal essential medium (MEM), which is a defined medium for mammalian cells. Both **S16** and **S32** exhibited at least four times lower MBC values (<0.19 μ M) against all bacterial species tested in MEM compared with MHB. In MHB, SNAPPs were found to aggregate to form particles with average D_H values of ~ 224.2 nm or greater, which is significantly larger in size than SNAPPs in MEM ($D_H = 7.7$ and 13.5 nm for **S16** and **S32**, respectively) (Supplementary Figs 6 and 7). Cryo-TEM images of **S16** in MHB further confirmed that the star formed large aggregates (~ 200 – 500 nm in diameter) (Supplementary Fig. 14). The formation of aggregates is consistent with previous studies that have reported that nutrient/ion-rich media often contain anionic peptide and protein fragments, which might bind non-specifically to cationic antimicrobials²⁷, thereby causing aggregation and the formation of larger-sized particles in MHB, as observed here. This postulation was validated as we observed a similar phenomenon where aggregates of **S16**, predominantly sized at 125 nm, were formed in 1% fetal bovine serum, another protein-rich medium (Supplementary Fig. 15). The aggregation of SNAPPs with the medium contents could possibly shield the active components of SNAPPs, thereby reducing their potency. Nevertheless, both **S16** and **S32** still possessed high efficacies in MHB, especially compared to the lead AMPs.

Biocompatibility of SNAPPs. As a test of biocompatibility, the haemolytic activities of SNAPPs were investigated by incubating them with red blood cells at different nanoparticle concentrations. Both **S16** and **S32** (as well as the control homolysine star) had

negligible haemolytic activity (>45 μ M, Supplementary Table 9). Even at a very high concentration of >100 \times MBC, the extent of haemolysis was well below 30% (Supplementary Fig. 16). Subsequently, we investigated the viability of two types of mammalian cells (human embryonic kidney (HEK293T) cells and rat hepatoma (H4IEE) cells) in response to SNAPPs. The therapeutic indices (TI) of SNAPPs ranged from 52 to 171 (Supplementary Table 10), generally higher than the TI of colistin²⁸, which is currently being used as the last therapeutic option for MDR Gram-negative pathogens²⁹.

In vivo efficacy of SNAPPs. The effectiveness of **S16** *in vivo* was evaluated in a mouse peritonitis model, where the intraperitoneal (i.p.) dose of *A. baumannii* (2×10^8 cells in MEM) resulted in the establishment of widespread bacterial infection by 24 h (Fig. 2a). At 0.5, 4 and 8 h post-infection, mice were treated with either MEM (control), the antibiotic imipenem (40 mg kg^{-1}) or **S16** (8.3 mg kg^{-1}). Similar to the imipenem-treated mice, treatment with **S16** resulted in >5-log reduction in bacterial cell counts in the peritoneal cavity (Fig. 2b), quantitative (>99%) eradication of bacterial cells in blood (Supplementary Fig. 17a) and >3-log colony forming unit (c.f.u.) reduction in the spleen (Supplementary Fig. 17b). Additionally, all mice treated with either imipenem or **S16** survived, with no signs of animal distress, whereas only 20% of the control/mock-treated mice survived after 24 h. A number of studies have found that antimicrobial agents enhance host cell innate immunity to bacteria *in vivo*³⁰; in this study, the **S16**-treated group had enhanced neutrophil infiltrate in the peritoneal cavity, while the imipenem-treated group did not show any significant difference from the mock-treated group (Fig. 2d).

As **S16** was effective *in vitro* against CMDR bacteria, we extended the peritonitis model by including the CMDR *A. baumannii*. Mice treated with **S16** had significantly less bacteria in the peritoneal cavity (Fig. 2c), blood (Supplementary Fig. 18a) and spleen (Supplementary Fig. 18b) and higher numbers of neutrophils in the peritoneal cavity (Fig. 2e) compared with the imipenem- and mock-treated groups. Imipenem treatment had no effect on reducing bacteria levels in all tissues examined, and this was comparable to the mock-treated group (Fig. 2c and Supplementary Fig. 18). All mice treated with **S16** survived with no signs of animal distress, but only 50% of the mock- or imipenem-treated mice survived the 24 h infection. The mechanism by which host defence peptides (HDPs) effect bacterial clearance *in vivo* is by neutrophil recruitment; however, unlike SNAPPs, HDPs often have poor direct antimicrobial activity³¹. **S16** has both direct (bacterial) and indirect (via neutrophil recruitment) antimicrobial activities *in vivo*. Although the CMDR *A. baumannii* isolate used herein has been found to acquire resistance against the last-resort drug, colistin³², these results demonstrated that **S16** is capable of treating CMDR *A. baumannii* and potentially other CMDR Gram-negative infections *in vivo*. To the best of our knowledge, this is the first report of a synthetic antimicrobial polymer having *in vivo* efficacy against a CMDR Gram-negative bacterial infection.

Preliminary mechanistic studies. To directly observe the interactions between an antimicrobial agent and bacterial cells, we conducted super-resolution fluorescence imaging using 3D structured illumination microscopy (3D-SIM). Sample images of untreated *E. coli* are provided in Fig. 3a and Supplementary Fig. 20a. Figure 3 shows the 3D-SIM images of *E. coli* (labelled red with lipid membrane FM4-64FX dye) incubated with the AF488-labelled **S16** (Supplementary Fig. 19 and Supplementary Table 11) in MHB at a dose approximately equivalent to 0.5 \times , 1 \times and 2 \times the MBC of the fluorescently tagged SNAPP (MBC_{tagged}). The action of antimicrobials on bacteria has been imaged using a range of microscopy techniques^{33,34}, but this is one of the first

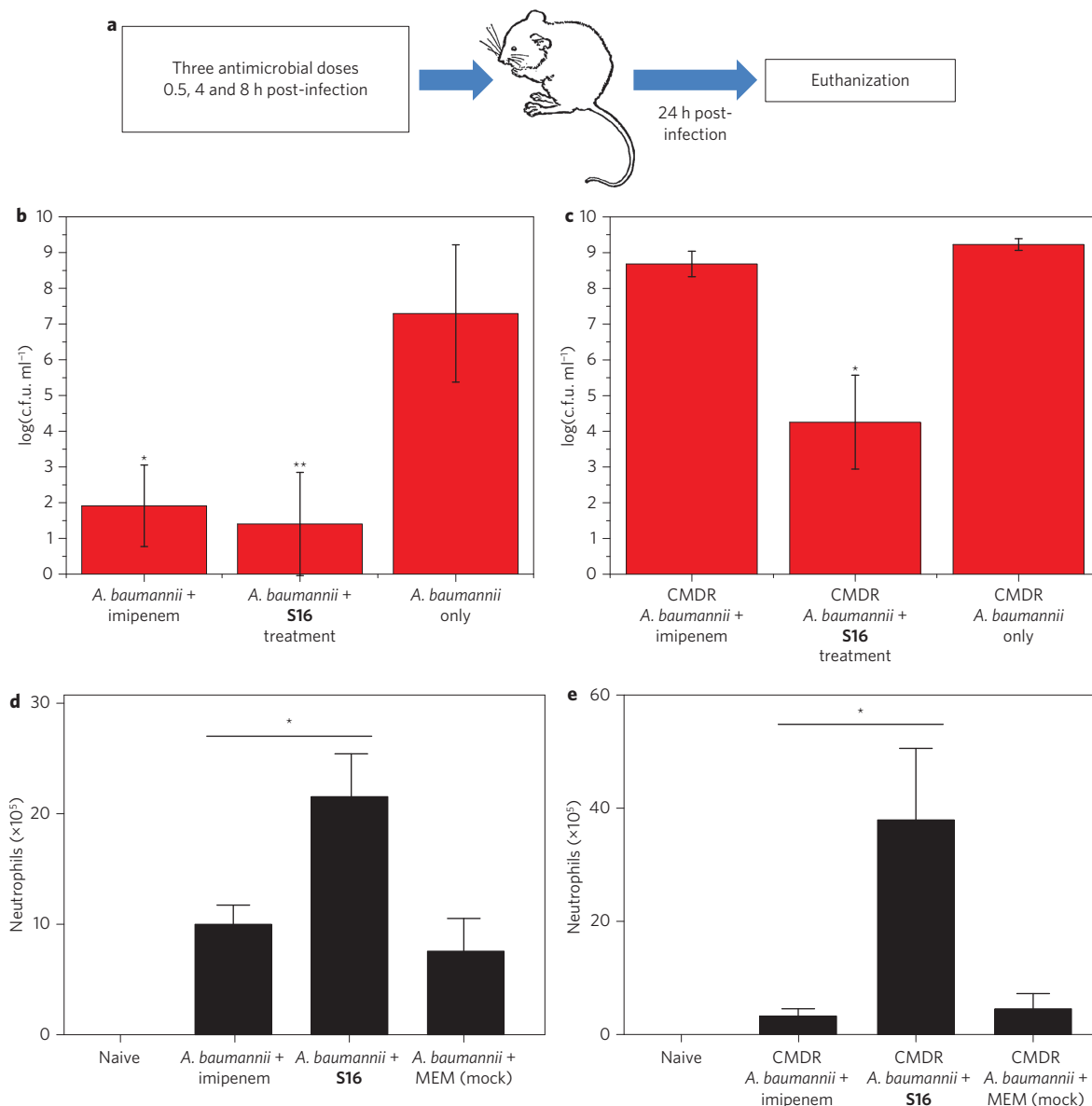


Figure 2 | In vivo efficacy of SNAPP S16 in a mouse peritonitis model. **a**, Schematic of the experimental protocol for the mouse peritonitis model. **b,c**, Colony forming units (c.f.u.) of *A. baumannii* (ATCC 19606) (**b**) and CMDR *A. baumannii* (FADDI-AB156) (**c**) found in the peritoneal wash of infected mice 24 h after mock (MEM) treatment or treatment with imipenem (40 mg kg^{-1}) or S16 (8.3 mg kg^{-1}). **d,e**, Numbers of peritoneal neutrophils in the mild peritonitis model with mice 24 h after infection with *A. baumannii* (ATCC 19606) (**d**) and CMDR *A. baumannii* (FADDI-AB156) (**e**) and either mock, imipenem (40 mg kg^{-1}) or S16 (8.3 mg kg^{-1}) treatments. All data are expressed as mean \pm s.d. (indicated by error bars), based on values obtained from five biological replicates ($n = 5$). * $P < 0.01$, ** $P < 0.001$, Student's t-test, significant difference from the mock (MEM) control group (**b,c**) and the imipenem-treated group (**d,e**).

instances where a clear visualization of the interaction between an antimicrobial agent and bacterial cells at the super-resolution level has been demonstrated. S16 (labelled green) was found to associate at certain sites on and in the bacteria depending on SNAPP concentration (Fig. 3b–h, Supplementary Figs 20 and 21 and Supplementary Videos 1 and 2). This is different to the membrane interactions of proline-rich AMPs, where the peptides localize uniformly around the *E. coli* membrane, as previously reported by us³⁵. At $0.5 \times \text{MBC}_{\text{tagged}}$, SNAPPs associate with the surface of the bacteria (Fig. 3b); however, at $1 \times \text{MBC}_{\text{tagged}}$, we observed a high density of bacterial cells with either membrane-associated or internalized star peptide polymers (Fig. 3c–e). On the other hand, in our previous study on membrane-lytic proline-rich AMPs, we observed complete internalization and uniform localization of peptides throughout the cytosol of the bacterial cells³⁵. We attributed this difference to the larger sizes of

SNAPPs, which possibly inhibited the quantitative internalization of all membrane-bound SNAPP macromolecules even when the membranes were disrupted. At $2 \times \text{MBC}_{\text{tagged}}$, there are clearly more membrane-associated or internalized SNAPPs per bacterial cell (Fig. 3f–h and Supplementary Fig. 20b–e). Orthogonal projections showed that the membrane-localized SNAPPs appear to aggregate and span the cell envelope (Supplementary Fig. 21). Furthermore, bacteria with internalized SNAPPs were observed to have distinct cell envelope perforations (Fig. 3h, Supplementary Figs 20d,e and 21b). When the experiments were conducted in MEM at $2 \times \text{MBC}_{\text{tagged}}$, the results were similar to those observed in MHB at supra-MBC dosage, albeit with a larger extent of SNAPP internalization into the cells (Supplementary Fig. 22).

Based upon the fluorescence imaging studies conducted, we hypothesized that SNAPPs initially localize on the bacterial OM as a result of electrostatic interactions. This could cause areas of

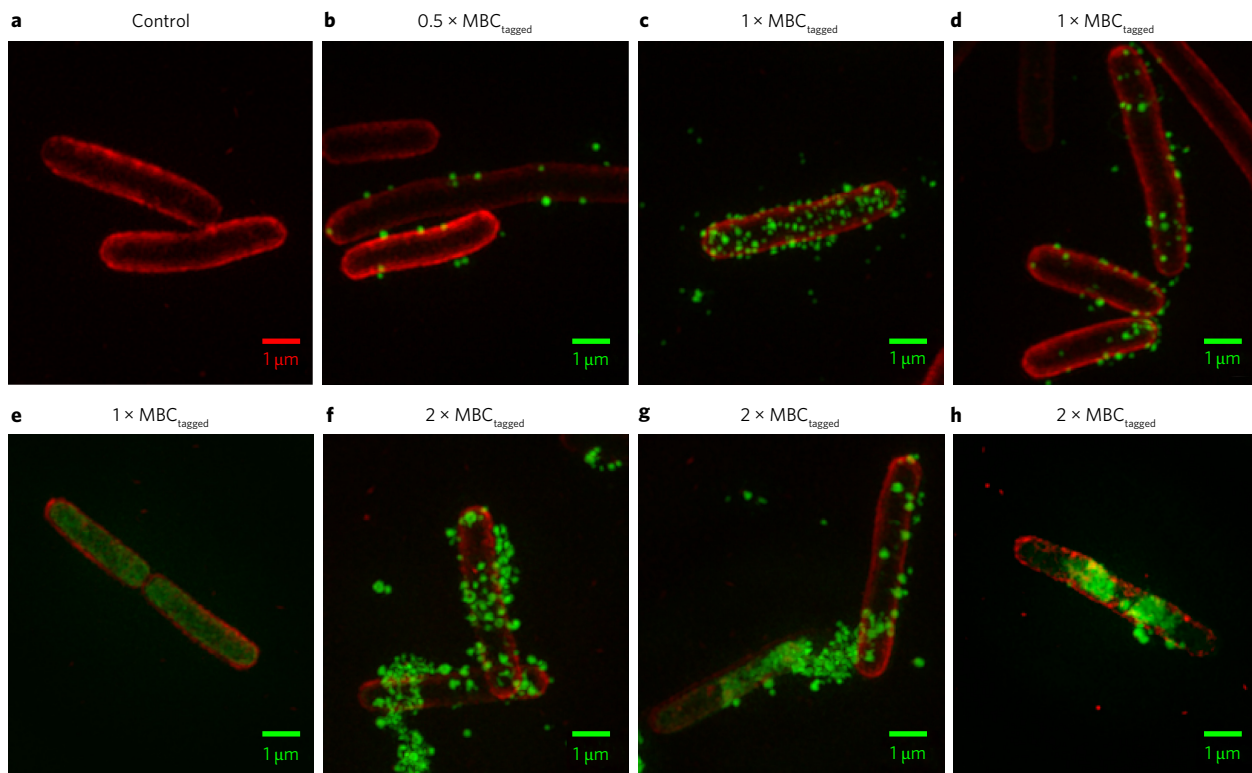


Figure 3 | Optical Microscope eXperimental 3D-SIM images of *E. coli* before and after treatment with AF488-tagged SNAPP S16 in MHB. **a–h**, Z-projection images of *E. coli* before (**a**) and after incubation with AF488-S16 at $0.5 \times \text{MBC}_{\text{tagged}}$ (**b**), $1 \times \text{MBC}_{\text{tagged}}$ (**c–e**) and $2 \times \text{MBC}_{\text{tagged}}$ (**f–h**). The *E. coli* cell membrane was stained with FM4-64FX (red) and S16 with AF488 (green) in all images. Note that the MBC used refers to the MBC of the fluorescently tagged SNAPP (Supplementary Table 11). All images are representative of three independent experiments.

destabilization/fragmentation, leading to SNAPPs possibly translocating to and disrupting the CM, thus leading to cell death³⁶. To investigate this hypothesis, we conducted a competitive inhibition assay with lipopolysaccharide (LPS). The co-incubation of LPS (from *E. coli*) with S16 was found to inhibit the ability of S16 to disrupt the membrane of *E. coli* cells in a dose-dependent manner (Supplementary Figs 23 and 24). This suggested that SNAPPs bind to LPS on the OM and could explain the selective antimicrobial activity of SNAPPs towards Gram-negative bacteria. However, as SNAPPs were still moderately active against the Gram-positive species tested, we postulate that the LPS-SNAPP interactions are preferred, due to the strong electrostatic interactions, but not highly specific to the extent where antimicrobial activity would be lost in the absence of LPS. Using flow cytometry, we demonstrated that the association of the AF488-tagged S16 with *E. coli* was linearly correlated with bacterial membrane disruption (Supplementary Figs 25 and 26). Furthermore, a time-course study showed that the action of S16 was rapid, as >90% of an *E. coli* cell population had disrupted membranes within 30 min, which correlated with complete population death (Supplementary Fig. 27). This fast kinetics of killing is similar to that observed for AMPs (ref. 37), which is most likely a distinctive feature of membrane-disruptive antimicrobials.

To investigate whether SNAPP-induced membrane disruption is a result of pore formation, as is the case with some AMPs, we conducted a dye release assay using dextran-loaded large unilamellar vesicles (LUVs) as a mimic for Gram-negative CM (ref. 38). The results suggested that SNAPPs do not cause membrane disruption via pore formation (Supplementary Fig. 28a). Another mechanism of membrane disruption is through unregulated ion movement, which we investigated using the LUV chloride ion (Cl^-) transport assay³⁹. Cl^- ion efflux was found to increase with increasing concentrations of S16 (Supplementary Fig. 28b). Additionally, we

performed membrane potential measurements on bacterial cells to determine the ability of SNAPPs to alter the membrane potential. It was observed that the treatment of *E. coli* cells with S16 induced mixed hyperpolarized and depolarized bacterial cell populations, with a shift towards a more depolarized population as concentration increased (Supplementary Figs 29 and 30). Taken together, these studies suggest that the interaction of SNAPPs with the CM may result in membrane perturbations that lead to unregulated ion movement and membrane potential dissipation.

A number of recent studies have shown that bacteria, like eukaryotic cells, have mechanisms of programmed cell death (PCD) that could be triggered under stressful conditions, such as membrane disruption^{40,41}. Two major PCD pathways have been described in bacteria: (1) the ALD pathway mediated by *recA* and *lexA* genes and (2) the *mazEF* pathway^{40,41}. Based on gene expression studies, S16 at $1 \times \text{MBC}$ induced a ten- and sevenfold increase in *recA* and *lexA*, respectively, but no change in *mazEF* levels (Supplementary Fig. 31). These results, when observed under cell death conditions, suggested that S16 induced ALD responses in *E. coli*. We also observed the production of reactive oxygen species (ROS) following S16 treatment (Supplementary Fig. 32), which has been reported to be a characteristic of ALD (ref. 42). The induction of ALD in bacteria has been reported in previous studies to lead to cell lysis⁴². We also found that when ALD was inhibited by pre-treating *E. coli* with a translation inhibitor (doxycycline), the antimicrobial activity of S16 remained comparable to that when ALD was not inhibited (Supplementary Fig. 33). This suggested that the induction of the ALD pathway is not a prerequisite for SNAPP activity, but is likely to be either an event that coincides with early membrane disruption or a supplementary (but not essential) bactericidal mechanism. At $5 \times \text{MBC}$, S16 induced significantly less *recA* and *lexA* mRNA than that at $1 \times \text{MBC}$ concentration

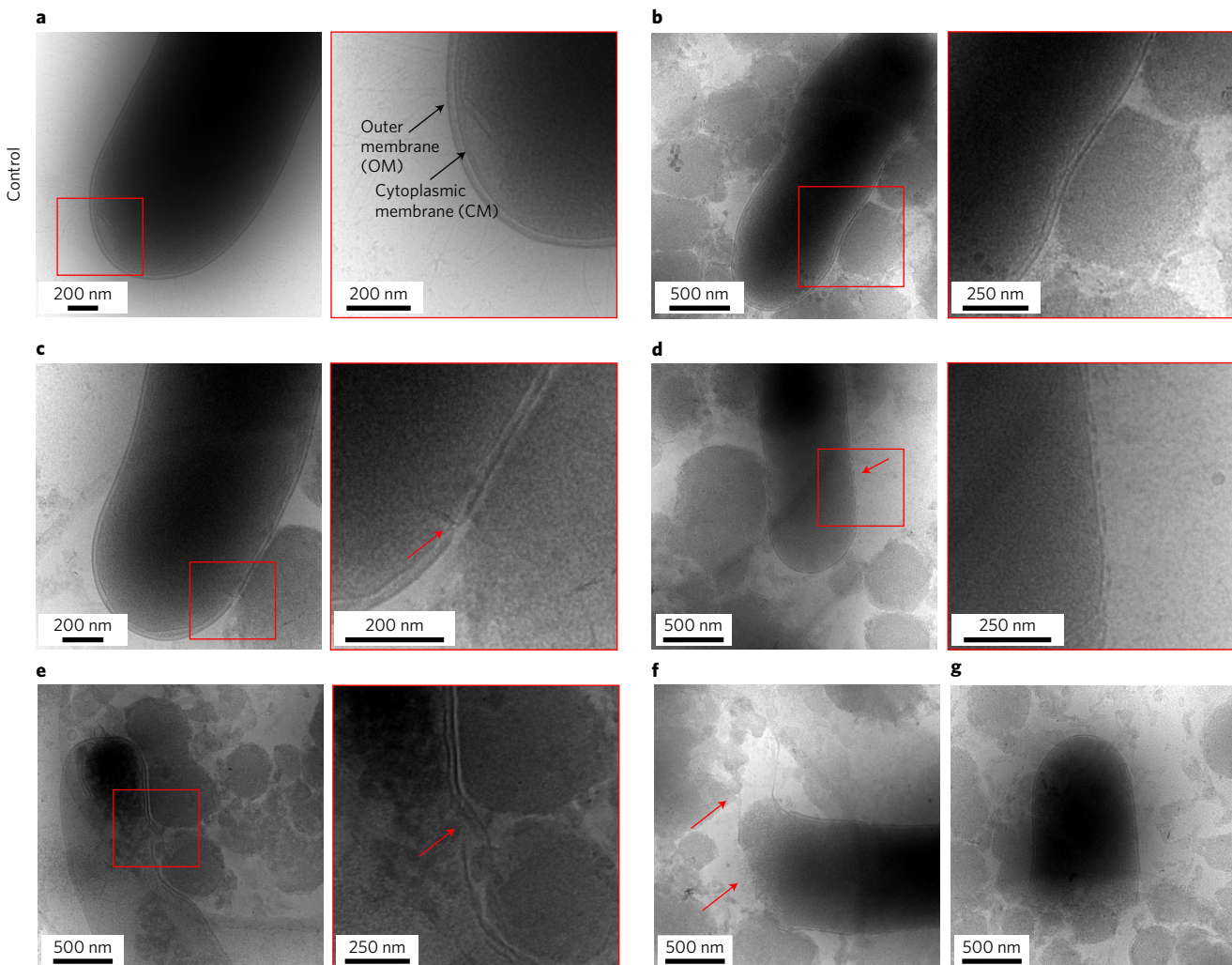


Figure 4 | Morphological studies of *E. coli* before and after treatment with S16 in MHB. **a–g**, Cryo-TEM images of *E. coli* before (**a**) and after incubation with S16 for 90 min at a lethal dose of $35 \mu\text{g ml}^{-1}$ ($1 \times \text{MBC}$ of the unlabelled S16 in MHB) (**b–g**). Large aggregates (possibly aggregates of S16 with medium contents) were observed around the rod-shaped *E. coli* cells (**b–g**). Binding of the aggregates to *E. coli* was observed and the cell membrane appeared disrupted (**b**). Hole formation (**c**), OM fragmentation (**d**), stripping of cell walls and membranes (**e**), ripping of cell ends (**f**) and isolated cell fragments (**g**) were observed. Enlarged images of **a–e** are provided and the sections enlarged are outlined in red. Scale bars, 200 nm, 250 nm or 500 nm as indicated. Regions of interest are indicated by red arrows. All images are representative of three independent experiments.

(Supplementary Fig. 31). We speculate that at supra-MBC dosage, other killing mechanisms would dominate, thus leading to insufficient time for the expression of ALD pathway components. This agreed with our previous postulation that there might be multiple mechanisms involved in the antimicrobial action of SNAPPs.

Next, we used cryo-TEM to visualize the effect of SNAPP treatment on *E. coli* cell morphology. Before treatment, all cells showed intact OMs and CMs (Fig. 4a and Supplementary Fig. 34a–c). After treatment with S16 in MHB at its MBC, large aggregates—probably formed by aggregation between S16 and media contents (*vide supra*)—were observed around the cells (Fig. 4b–g and Supplementary Fig. 34d–g). The cell membranes of bacteria incubated with S16 appeared disrupted (Fig. 4b) and had pores that traversed the OM, peptidoglycan (PG) layer and CM (Fig. 4c and Supplementary Fig. 34d). Most bacterial cells had fragmented or perforated OMs (Fig. 4d,e and Supplementary Fig. 34e,f) and some cells appeared to be broken into isolated fragments (Fig. 4g and Supplementary Fig. 34g). These observations were in agreement with the flow cytometry data, which indicated that SNAPP association leads to membrane disruption. Cryo-TEM experiments conducted in MEM at supra-MBC dosage resulted in observations similar to when

MHB was used at similar dosages; however, more drastic cell lysis was noted in the case of MEM (Supplementary Fig. 35).

Taken together, we postulate that SNAPPs have a multimodal mechanism of inducing bacterial cell death. Initially, SNAPPs bind via electrostatic interactions with LPS and the OM, leading to destabilized/fragmented areas. They then assemble and traverse the cell envelope driven by the transmembrane electrical potential (the interior/cytosol being negative), most probably causing membrane perturbations that result in unregulated transmembrane ion movement in the CM. These membrane disruption events induce ALD at low SNAPP concentrations, thus leading to cell lysis⁴². At high concentrations, SNAPPs rapidly cause cell lysis by direct disruption of the OM and CM. Collectively, fluorescence imaging, flow cytometry and cryo-TEM assays provided evidence for membrane association, membrane disruption, OM fragmentation/destabilization and cell lysis. Although the exact sequence of events requires further investigations, we can conclude that the succession of antimicrobial events, as depicted in Fig. 5, is substantially different from the action of a monomeric cationic AMP. A typical monomeric AMP is commonly thought to traverse the OM of a Gram-negative bacterial cell via self-promoted uptake, binds to

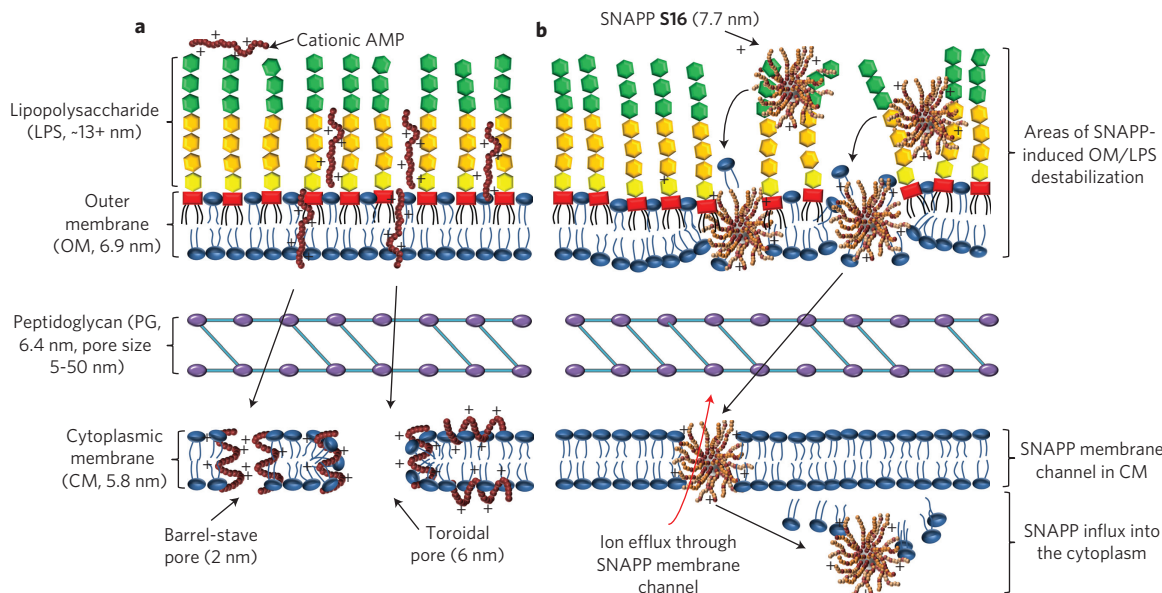


Figure 5 | A comparison between the antimicrobial mechanism(s) of typical membrane-disrupting cationic AMPs and the possible mechanism of SNAPPs against Gram-negative bacteria. **a**, Cationic AMPs bind to the OM of Gram-negative bacteria via electrostatic interactions, transit across the OM through membrane destabilization and disrupt the physical integrity of the CM by the ‘barrel-stave’, ‘toroidal-pore’ or ‘carpet’ pore (not shown in figure) mechanisms¹⁸. **b**, SNAPPs, whether in their aggregated or unaggregated state, interact with the OM, PG and CM layers of Gram-negative bacteria via electrostatic attractions and kill the cell by fragmenting/destabilizing its OM and possibly disrupting the CM such that unregulated ion movement results, but also by the induction of the apoptotic-like death pathway (not shown in figure), thereby lysing the cell.

and inserts itself into the anionic surface of the CM, then kills the bacteria by either membrane disruption (pore formation) or translocation across the CM and acting on internal targets^{12,43,44}. In the case where cell death is caused by membrane disruption, loss of CM integrity was commonly thought to be the lethal event^{12,45,46}. Cryo-TEM analysis of *E. coli* after incubation with melittin or ovispirin (which are well-characterized AMPs) confirmed that the AMPs disrupted the CM while leaving the OM intact (Supplementary Fig. 36). On the other hand, as demonstrated here, it is likely that **S16** effects its antimicrobial action in a cascade manner and by first disrupting the physical integrity of the OM upon binding with LPS. We hypothesize that the difference in the mode of action between monomeric cationic AMPs and **S16** might be attributed to the latter’s structural architecture, as SNAPPs might be unable to translocate across the OM and CM without causing significant perturbation.

AMPs as a whole class of compounds kill bacteria by multiple mechanisms, but each specific AMP tends to kill bacteria by one major mechanism⁸. The multifaceted interactions shown here between SNAPPs and bacteria (in combination with indirect antimicrobial activity via neutrophil recruitment *in vivo*) are truly unique and this, to the best of our knowledge, has not been shown previously in a definitive manner for any one single AMP. Silver ions have been shown to enhance antibiotic activity by interacting with several cytosolic molecules, which corroborates our data suggesting that an antimicrobial agent may have more than one mode of action⁴⁷. The equipotency of SNAPPs against all of the Gram-negative bacteria tested suggested that the multimodal mechanism of action is non-specific, and we postulate that this is why bacteria did not acquire resistance to star **S16**, even after 600 generations of growth in the presence of the agent. The successful demonstration of the antimicrobial efficacy of SNAPPs against CMDR *A. baumannii* *in vivo* as well as their biocompatibility will undoubtedly distinguish SNAPPs as a new class of antimicrobial agents, potentially capable of addressing the dearth of suitable drug candidates to combat Gram-negative pathogens resistant to conventional antibiotics.

Methods

Synthesis of L-lysine(Z)-NCA (Lys NCA). Dried H-Lys(Z)-OH (1.24 g, 4.43 mmol) was added to anhydrous THF (25 ml) in an oven-dried two-necked round-bottomed flask under argon. Triphosgene (580 mg, 1.96 mmol) was dissolved in anhydrous THF (5 ml) and added to the H-Lys(Z)-OH suspension. The mixture was heated at 50 °C for 30 min with continuous stirring. The clear solution was allowed to cool to room temperature and added to anhydrous pentane (100 ml). The resulting precipitate was isolated via centrifugation and washed with anhydrous pentane (30 ml × 2). The resulting white solid was dried at ambient temperature *in vacuo* to afford Lys NCA, 0.910 g (81%). ¹H NMR (400 MHz, *d*₆-DMSO) δ_H 1.23–1.37 (m, γ-CH₂, 2H), 1.37–1.45 (m, δ-CH₂, 2H), 1.60–1.80 (m, β-CH₂, 2H), 2.94–3.02 (m, ε-CH₂, 2H), 4.40–4.43 (m, α-CH, 1H), 5.00 (dd, C₆H₅CH₂-, 2H), 6.90 (s, cyclic NH, 1H), 7.30–7.39 (m, C₆H₅-, 5H).

Synthesis of DL-valine-NCA (Val NCA). Dried DL-valine (1.24 g, 4.43 mmol) was dissolved in anhydrous THF (25 ml) in an oven-dried two-necked round-bottomed flask under argon. Triphosgene (580 mg, 1.96 mmol) was dissolved in anhydrous THF (5 ml) and added to the DL-val-THF suspension. The mixture was heated at 50 °C for 30 min with continuous stirring. The clear solution was allowed to cool to room temperature and precipitated with anhydrous pentane (100 ml), followed by washing with more anhydrous pentane (30 ml × 2). The resulting residue was dried at ambient temperature *in vacuo* to afford Val NCA, 0.956 mg (85%). ¹H NMR (400 MHz, *d*₆-DMSO) δ_H 0.91 (dd, CH₃, 6H), 2.00–2.12 (m, CH, 1H), 4.32 (dd, cyclic CH, 1H), 9.06 (s, cyclic NH, 1H).

Synthesis of poly(Z-L-lysine-*r*-DL-valine)_{arm}PAMAM-(NH₂)_{16,core} star peptide polymer S16_Z. Lys NCA (1.3 g, 4.19 mmol) and Val NCA (0.3 g, 2.1 mmol) were dissolved in anhydrous DMF (16 ml) and added via syringe to PAMAM-(NH₂)₁₆ (dried, 43 mg, 13.1 μmol) dissolved in anhydrous DMF (1 ml). After stirring for 24 h under argon, *n*-butyl alcohol (1 ml) was added and the mixture was stirred for a further 1 h. Precipitation of the concentrated peptide polymer solution into diethyl ether (3 × 40 ml), followed by isolation via centrifugation and drying (0.1 mbar), afforded (PZLL-*r*-PVAl)_{arm}PAMAM-(NH₂)_{16,core} star peptide polymer **S16_Z** as an off-white solid, 1.21 g (90%). ¹H NMR (400 MHz, *d*₆-DMSO) δ_H 0.67–0.89 (b, CH₃, 6H), 1.11–1.77 (b, γ-CH₂ + δ-CH₂ + β-CH₂, 6H), 1.84–2.00 (b, CH, 1H), 2.78–3.00 (b, ε-CH₂, 2H), 4.06–4.40 (b, α-CH, 1H), 4.90–5.00 (b, C₆H₅CH₂-, 2H), 7.00–7.44 (b, C₆H₅-, 5H), 7.60–8.30 (b, NH, 1H).

Synthesis of poly(Z-L-lysine-*r*-DL-valine)_{arm}PAMAM-(NH₂)_{32,core} star peptide polymer S32_Z. Lys NCA (1.3 g, 4.19 mmol) and Val NCA (0.3 g, 2.1 mmol) were dissolved in anhydrous DMF (16 ml) and added via syringe to PAMAM-(NH₂)₃₂ (dried, 43 mg, 13.1 μmol) dissolved in anhydrous DMF (1 ml). After stirring for 24 h under argon, *n*-butyl alcohol (1 ml) was added and the mixture was stirred for a further 1 h. Precipitation of the concentrated peptide polymer solution into diethyl

ether (3×40 ml), followed by isolation via centrifugation and drying (0.1 mbar), afforded (PZLL-*r*-PVal)₃₂PAMAM-(NH₂)₃₂core star peptide polymer S32_Z as an off-white solid, 1.15 g (85%). ¹H NMR (400 MHz, d_6 -DMSO) δ_{H} 0.67–0.89 (b, CH₃, 6H), 1.11–1.77 (b, γ -CH₂ + δ -CH₂ + β -CH₂, 6H), 1.84–2.00 (b, CH, 1H), 2.78–3.00 (b, ϵ -CH₂, 2H), 4.06–4.40 (b, α -CH, 1H), 4.90–5.00 (b, C₆H₅CH₂-, 2H), 7.00–7.44 (b, C₆H₅, 5H), 7.60–8.30 (b, NH, 1H).

Synthesis of linear poly(Z-L-lysine-*r*-DL-valine) peptide polymer L_Z. Lys NCA (0.5 g, 1.63 mmol) and Val NCA (117 mg, 0.82 mmol) were dissolved in anhydrous DMF (6 ml) and added via syringe to 4-methylbenzylamine (10.3 μ l, 80.9 μ mol). After stirring for 24 h under argon, *n*-butyl alcohol (1 ml) was added and the mixture was stirred for a further 1 h. Precipitation of the concentrated peptide polymer solution into diethyl ether (3×40 ml), followed by isolation via centrifugation and drying (0.1 mbar), afforded linear PZLL-*r*-PVal peptide polymer L_Z as an off-white solid, 420 mg (81%). ¹H NMR (400 MHz, d_6 -DMSO) δ_{H} 0.67–0.89 (b, CH₃, 6H), 1.11–1.77 (b, γ -CH₂ + δ -CH₂ + β -CH₂, 6H), 1.84–2.00 (b, CH, 1H), 2.78–3.00 (b, ϵ -CH₂, 2H), 4.06–4.40 (b, α -CH, 1H), 4.90–5.00 (b, C₆H₅CH₂-, 2H), 7.00–7.44 (b, C₆H₄-, 4H), 7.60–8.30 (b, NH, 1H).

General procedure for deprotection of peptide polymers. The peptide polymer was dissolved in TFA (200 mg ml⁻¹) and 33% HBr in acetic acid was then added (20 ml g⁻¹ peptide polymer). After 24 h stirring at room temperature, the mixture was precipitated into diethyl ether (ten times the volume of the reaction). The precipitate was isolated via centrifugation, redissolved in hydrochloric acid solution (0.2 M, 0.2 ml mg⁻¹ peptide polymer) and dialysed against RO water for 4 days. The dialysed solution was lyophilized to obtain the deprotected SNAPP (for example, S16 and S32). **S16 and S32:** ¹H NMR (400 MHz, d_6 -DMSO) δ_{H} 0.67–0.88 (b, CH₃, 6H), 1.05–1.77 (b, γ -CH₂ + δ -CH₂ + β -CH₂, 6H), 1.84–2.00 (b, CH, 1H), 2.61–2.83 (b, ϵ -CH₂, 2H), 4.00–4.39 (b, α -CH, 1H), 7.60–8.30 (b, NH, 1H). **L:** ¹H NMR (400 MHz, d_6 -DMSO) δ_{H} 0.67–0.88 (b, CH₃, 6H), 1.05–1.77 (b, γ -CH₂ + δ -CH₂ + β -CH₂, 6H), 1.84–2.00 (b, CH, 1H), 2.61–2.83 (b, ϵ -CH₂, 2H), 4.00–4.39 (b, α -CH, 1H), 7.00–7.20 (b, C₆H₄-, 4H), 7.60–8.30 (b, NH, 1H).

Synthesis of AMPs (ovispirin, magainin II and melittin). Ovispirin (NH₂-KNLRRRIIRKIIHIKKYKG-COOH), magainin II (NH₂-GIGKFLHSAAKKFGKAFTVGEMINS-CONH₂) and melittin (NH₂-GIGAVLKVLTTGLPALISWIKRKRQQ-CONH₂) were chemically synthesized on a CEM Liberty microwave peptide synthesizer (Ai Scientific). The peptide-resins were assembled from Fmoc-Rink-AM SURE resin in the Fmoc/TBu mode of synthesis. For a 0.1 mmol reaction scale, Fmoc-deprotection was performed in two stages by initial treatment with 20% piperidine/0.1 M HOEt/DMF (vol/vol, 7 ml) under microwave radiation for 30 s (40 W, 40 °C), followed by filtration and a second addition of the above solution (45 W, 75 °C; 3 min). The peptide-resins were then rinsed with DMF (4 \times 7 ml). Acylation, where required, was achieved by the addition of a solution containing amino acid (5 equiv., relative to reaction scale), 2-(1H-benzotriazol-1-yl)-1,1,3,3-tetramethyluronium hexafluorophosphate (HBTU) (5 equiv.) and *N,N*-disopropylethylamine (DIEA) (10 eq) in DMF/NMP (7:1, vol/vol; 4 ml) to the Na^+ -deprotected peptide-resin, and the mixture was agitated under microwave radiation for 10 min (30 W, 75 °C, vessel under external chilled air flow). Dichloromethane (DCM) (5 \times 2 min) was used to rinse the peptide-resins before the cleavage step. The peptide was cleaved from the resin support by the addition of TFA/triisopropylsilane (TIPS)/thioanisole/phenol/water (90:2.5:2.5:2.5, % vol/vol/vol/vol; 5 ml) for 2.5 h, after which the combined cleavage filtrates were evaporated under nitrogen flow and the crude product was isolated by precipitation in cold ether (4 \times 30 ml).

The crude peptide was purified using an Agilent 1200 series liquid chromatograph instrument (Agilent) equipped with an ultraviolet detector (model G1316A) and a Zorbax 300 SB-C18 reversed phase column (9.4 mm \times 25 cm). Crude peptide analysis was achieved using a linear acetonitrile gradient in 0.1% TFA at a flow rate of 4 ml min⁻¹ (linear gradient of 0–54% CH₃CN over 15 min). Analysis of the purified peptide was performed using an Esquire HCT electrospray ionization-mass spectrometry system (Bruker Daltonics).

Bacterial cell culture. Freeze-dried cultures of *E. coli* (ATCC 25922), *K. pneumoniae* (ATCC 13883), *A. baumannii* (ATCC 19606), colistin and multi-drug resistant (CMDR) *A. baumannii* (FADDI-AB156), CMDR *P. aeruginosa* (FADDI-PA067) and *S. aureus* (ATCC 29213) were grown aerobically and maintained by passage at ambient temperature on horse blood agar (10% vol/vol defibrinated horse blood, 4.4% wt/vol Oxoid Blood Agar Base No. 2). *P. aeruginosa* (ATCC 47085) were cultured in a similar fashion, except at 37 °C. Freeze-dried cultures of *S. mutans* (Ingbritt strain) were grown anaerobically and maintained by passage at 37 °C on Todd Hewitt agar (3.6% wt/vol Oxoid Todd-Hewitt Broth, 1.5% wt/vol sucrose, 1.5% wt/vol Bacto agar, 0.8% wt/vol Oxoid yeast extract). For *E. coli*, *K. pneumoniae*, *P. aeruginosa*, CMDR *P. aeruginosa*, *A. baumannii*, CMDR *A. baumannii* and *S. aureus*, overnight cultures were made by transferring a colony (~half a loop) from the agar plates to culture tubes containing sterilized Luria-Bertani broth (LB, 1% wt/vol bacto tryptone, 1% wt/vol NaCl, 0.5% wt/vol Oxoid yeast extract) (20 ml). Bacterial cultures were incubated overnight at 37 °C with aeration and without agitation, with the exception of CMDR *P. aeruginosa*, which was cultured at

37 °C with aeration and agitation (150 r.p.m.). The next day, for *E. coli*, *K. pneumoniae*, *P. aeruginosa*, CMDR *P. aeruginosa* and *S. aureus*, small aliquots (that is, 0.5–2 ml) were taken from the culture tubes, further diluted with LB (20 ml), and incubated for 3–4 h at 37 °C with aeration before use. All bacterial cultures were cultured without agitation, with the exception of *P. aeruginosa* and CMDR *P. aeruginosa*, which were cultured with shaking at 150 r.p.m. For *A. baumannii*, an aliquot of 0.5 ml was taken from the overnight culture tube, further diluted with LB (200 ml) and incubated overnight at 37 °C with aeration before use. With regards to *S. mutans*, several colonies (~half a loop) from the agar plates were transferred to culture tubes containing sterilized Todd Hewitt broth (3.6% wt/vol Oxoid Todd Hewitt broth, 1.5% wt/vol sucrose, 0.8% wt/vol Oxoid yeast extract) (20 ml). The cultures were incubated overnight at 37 °C in the anaerobic chamber. After 24 h, a small aliquot (that is, 0.5 ml) was taken from the culture tubes, further diluted with media (~200 ml) and incubated overnight at 37 °C in the anaerobic chamber before use.

Bacterial cell counting. A Cell Lab Quanta SC MPL flow cytometer was used to count the number of bacterial cells before use in assays. Cells were diluted with saline using an appropriate dilution factor and incubated with Syto 9 and propidium iodide (PI) (that is, 1 ml cell solution to 1 μ l of each dye). Syto 9 stains the nucleic acids in all cells, while PI stains the nucleic acids in cells with damaged membranes. Using the Cell Lab Quanta SC software, the number of viable cells per ml (Syto 9-positive, PI-negative) was obtained.

Measurement of MBC. A dilution series of each compound was made by diluting test compound stock in media to a desired range of concentrations and a final volume of 100 μ l in each well of a 96-well plate. Bacterial cells (which gave an optical density (OD) reading of ~0.7 at 650 nm for *E. coli*, *K. pneumoniae*, *P. aeruginosa* and *S. aureus*, ~0.5 at 650 nm for *A. baumannii* and ~1.8 at 650 nm for *S. mutans*) were diluted to 2.5×10^6 cells ml⁻¹ in media, and 100 μ l of the bacteria solution was added to each well. The 96-well plate was then incubated at 37 °C for 90 min. For each well, microbial solution was diluted with saline (0.9% NaCl solution) using an appropriate dilution factor and placed on an agar plate (identical to that used for bacteria culture). For *E. coli*, *K. pneumoniae*, *A. baumannii* and *S. aureus*, the agar plates were incubated overnight at room temperature and then at 37 °C with aeration for 2 h. For *P. aeruginosa* and *S. mutans*, the agar plates were incubated at 37 °C, with the former being incubated overnight with aeration and the latter in an anaerobic chamber for 48 h. The numbers of c.f.u. were counted and expressed as c.f.u. ml⁻¹. Positive controls consisting of cells without any treatment were used. Concentration-killing curves were plotted with c.f.u. ml⁻¹ as a function of compound concentration, and linear regression analysis was used to determine the lowest concentration (MBC) at which the c.f.u. ml⁻¹ becomes zero (Supplementary Fig. 9). A minimum of two independent experiments (biological replicates) of the assay were conducted, and two technical replicates were used in each experiment for each bacterium, compound and concentration. Data are expressed as mean \pm standard deviation (s.d.) of the biological replicates and analysed using Student's *t*-test. Note that for *E. coli*, *K. pneumoniae*, *P. aeruginosa* and *A. baumannii*, two sets of experiments were performed, either using a nutritionally rich medium (MHB, 3.8% wt/vol Oxoid Mueller-Hinton agar) or MEM (136.9 mM NaCl, 10.1 mM Na₂HPO₄, 2.7 mM KCl, 1.8 mM KH₂PO₄, 0.2% wt/vol d-(+)-glucose). For *S. aureus* and *S. mutans*, the assays were conducted in nutritionally rich media only (Luria-Bertani broth and Todd-Hewitt broth, respectively).

Measurement of MIC. The MIC values of the PAMAM dendrimers were determined using a broth microdilution method. After the preparation of a dilution series of each compound and the addition of bacterial cells (note: the steps are identical to those taken for the measurement of MBC), the optical density readings of each well at 630 nm were measured as a function of time using a microplate reader (Multiskan Ascent, PathTech). Positive controls containing cells alone were incorporated. Optical density was plotted against polymer concentration, and linear regression analysis was used to determine the lowest concentration (MIC) at which the optical density reading becomes zero. A minimum of two independent experiments (biological replicates) of the assay were conducted, and two technical replicates were used in each experiment for each bacterium, polymer and concentration. Data are expressed as mean \pm s.d. of the biological replicates and analysed using Student's *t*-test.

Resistance studies. The method used was adapted from that of Gullberg and co-authors⁴⁸. Overnight cultures of *A. baumannii* cells (ATCC 19606 or FADDI-AB156) in LB broth were obtained from independent colonies grown on horse blood agar. The cells were then serially passaged by 400-fold dilution in 1 ml batch cultures every 24 h for 600 generations (~25 generations of growth per serial passage) in MHB containing 1/10 of the MBC of S16 (for both strains). After every 100 generations of growth, the MBCs of S16 were obtained using cells that were serially passaged in the presence of the antimicrobial agent. As a control, MBCs were also obtained using cells serially passaged in fresh MHB alone.

Haemolysis assay. Fresh sheep red blood cells (RBCs) were diluted 1:20 in PBS (pH 7.4), pelleted by centrifugation and washed three times in PBS (1,000g, 10 min). The RBCs were counted using a cell counter (Coulter Particle Counter Z series,

Beckman Coulter) and diluted to a final concentration of 2×10^7 cells ml $^{-1}$. Aliquots (100 μ l) of the RBC solution were seeded into a V-bottomed 96-well plate containing 100 μ l of test compound solution of varying concentrations (4–2,000 μ g ml $^{-1}$) and incubated in a humidified atmosphere containing 5% CO $_2$ at 37 °C for 2 h. Following incubation, the 96-well plate was centrifuged (1,000g, 10 min) and aliquots (100 μ l) of supernatant were transferred to a flat-bottomed 96-well plate. Haemoglobin release upon lysis of the RBCs was monitored at 405 nm using a microplate reader (PerkinElmer 1420 Multilabel Counter VICTOR 3). Positive and negative controls for haemolysis were taken as RBCs lysed with 0.5% Triton X-100 (1:1 vol/vol) and RBC suspension in PBS, respectively. The percentage of haemolysis was calculated using the formula

$$\% \text{ Haemolysis} = \left(\frac{A_{405} \text{ test sample} - A_{405} \text{ negative control}}{A_{405} \text{ positive control} - A_{405} \text{ negative control}} \right) \times 100$$

The percent haemolysis was plotted against peptide polymer concentration, and linear regression analysis was used to determine the haemolytic concentration needed to lyse 50% (HC $_{50}$) of RBCs. Two independent runs of the assay were conducted and two replicates were used in each run for each compound and concentration.

Mammalian cell culture. Human embryonic kidney cells (HEK293T) were cultivated in ‘complete’ RPMI-1640 medium (supplemented with 5% FBS, 1 \times GlutaMAX, 1 \times antibiotic-antimycotic and 1 \times MEM non-essential amino acids) in a humidified atmosphere containing 5% CO $_2$ at 37 °C. Cells were seeded in a T75 flask ($\sim 3 \times 10^6$ cells ml $^{-1}$) and passaged twice a week before performing subsequent cell viability studies. Rat hepatoma cells (H4IIE) were cultivated in DMEM medium (supplemented with 10% FBS, 1 \times GlutaMAX and 1 \times penicillin-streptomycin) in a humidified atmosphere containing 5% CO $_2$ at 37 °C. Cells were seeded in a T75 flask ($\sim 3 \times 10^6$ cells ml $^{-1}$) and passaged twice a week before performing subsequent cell viability studies.

Apoptosis/necrosis assay. Adherent HEK293T or H4IIE cells (obtained from the ATCC and throughout the course of the study were checked for mycoplasma contamination using the Mycoplasma stain kit Myc1, Aldrich) were grown to 80% confluence and trypsinized before assay. HEK293T and H4IIE cells were chosen for this study as they are standard cell lines used in toxicity studies. Cells were diluted 1:2 with ‘complete’ medium (RPMI-1640 for HEK293T cells or DMEM for H4IIE cells) and seeded in a 24-well plate (1 ml per well). The cells were incubated at 37 °C in 5% CO $_2$ for 24 h until \sim 95% confluence. The medium was removed. Varying concentrations of test compound (4–128 μ g ml $^{-1}$) were prepared, and 200 μ l aliquots of each were added to the cells, after which the cells were incubated at 37 °C in 5% CO $_2$ for 90 min. The cells were then collected and all well contents were transferred to round-bottomed polypropylene tubes (5 ml). The cells were washed with cold Dulbecco’s phosphate-buffered saline (DPBS), then stained with YO-PRO-1 and PI (0.2 ml from a stock solution, whereby both dyes were diluted 1:1,000 in cold DPBS, per well) and incubated on ice for 20–30 min. The cells were analysed by flow cytometry (Cyomics FC 500 MPL System). Standard compensation was performed using single-colour stained cells. Negative controls using untreated cells were included. Two independent runs of the assay were conducted, and two replicates were used in each run for each test compound and concentration.

In vivo efficacy of SNAPP S16. All experiments involving animals were performed according to protocols approved by the University of Melbourne Biochemistry and Molecular Biology, Dental Science, Medicine, Microbiology and Immunology, and Surgery Animal Ethics Committee (project no. 1513489). Ten- to 14-week-old female C57BL/6 mice (weighing 23.2 ± 1.7 g, animals under 20 g were not used in this study) were used in all *in vivo* studies, with five animals per group. Experiments were conducted without randomization or blinded protocol. Using preliminary peritonitis infection data and a power analysis (using SPSS for Windows, version 12), a sample size ≥ 2 would be needed to detect a large effect size ($d = 0.8$) with 95% power, using a *t*-test between means with alpha at 0.01. After 1 week of quarantine, inoculation ($t = 0$) was performed by i.p. injection of 300 μ l of 2×10^8 cells, delivered in MEM, of wild-type *A. baumannii* (ATCC 19606) or CMDR *A. baumannii* (FADDI-AB056) with a 25-gauge syringe. Two groups ($n = 5$ for ATCC 19606 and $n = 5$ for FADDI-AB056) received either SNAPP S16 (8.3 mg kg $^{-1}$ per dose in MEM, which corresponds to 1.5 \times *in vitro* MBC taking into account the average peritoneal/blood volume of mice) or imipenem (derived from the carbapenem antibiotic family and considered to be the most successful class of antibiotics in evading emerging antimicrobial resistance 49 , 40 mg kg $^{-1}$ per dose in MEM) treatment 0.5, 4 and 8 h after introduction of the inoculums. An untreated control group was included. Signs of animal distress were monitored and mice that did not meet distress-related euthanasia criteria at $t < 24$ h were defined as ‘survived’. At $t = 24$ h, all mice were euthanized. Peritoneal washes were performed by injecting 3.0 ml of sterile MEM in the intraperitoneal cavity followed by a massage of the abdomen. Subsequently, the abdomen was opened and 3.0 ml of peritoneal fluid was recovered from the peritoneum for analysis of c.f.u. ml $^{-1}$. Spleen of each mouse was

removed and suspended in 5.0 ml MEM in a gentleMACS tube, which was then subjected to automatic dissociation (gentleMACS dissociator, Miltenyi Biotec). The peritoneal fluid and supernatant from the dissociation of spleen were serially diluted in saline. A 10 μ l portion of each dilution was plated on horse blood agar plates and incubated overnight at 37 °C. For mice that were still alive directly before euthanasia, blood was also taken from the heart for immediate plating on horse blood agar plates. Colonies were counted and expressed as c.f.u. ml $^{-1}$, and viable bacteria cell counts in the peritoneal cavity (Fig. 2b,c), blood (Supplementary Figs 17a and 18a) and spleen (Supplementary Figs 17b and 18b) were compared with those of the control group at 24 h. The bacterial levels were statistically analysed using a one-way classification analysis of variance (ANOVA) and Student’s *t*-test (SPSS for Windows, version 12). Data are expressed as mean \pm s.d. of five biological replicates.

Fluorescent tagging of SNAPP S16 with Alexa Fluor 488. SNAPP S16 was dissolved in sodium bicarbonate buffer (0.1 M, pH 8.3) (2.5 mg ml $^{-1}$), and Alexa Fluor 488 (AF488) carboxylic acid succinimidyl ester dissolved in DMSO (10 mg ml $^{-1}$) was added (20 μ l mg $^{-1}$ of peptide polymer). The mixture was stirred for 1 h at room temperature and then passed through a gel separation column (PD MidiTrap G-25) to remove excess dye. The filtrate was lyophilized to afford the fluorescently tagged derivative, AF488-S16.

Sample preparation for imaging with 3D-SIM super-resolution microscopy. Sterilized chambered coverglasses were coated with poly-D-lysine (0.1 ml per well from a 0.1 mg ml $^{-1}$ stock solution in DPBS) for 90 min. The excess poly-D-lysine was removed by washing with sterilized MilliQ water (2 \times 0.5 ml) and the coverglasses were left to dry overnight in a sterile environment. *E. coli* cells (1.25×10^6 cells ml $^{-1}$, prepared as described for the measurement of MBC) were incubated with AF488-S16 (8–256 μ g ml $^{-1}$) in a 96-well plate at 37 °C for 90 min. The cell suspension was then transferred to Eppendorf tubes (2 ml) and washed with Hank’s balanced salt solution (HBSS) twice (5,000g, 10 min). FM 4-64FX dye (0.2 ml from a 5 μ g ml $^{-1}$ stock solution in HBSS) was added to the cell pellet and the cells were incubated on ice for 10 min with regular mixing. After incubation, the cells were washed with HBSS (5,000g, 10 min), resuspended in HBSS (0.5 ml) and then transferred to the chambered coverglass. Subsequently, the cells were washed in HBSS (800g, 10 min) then fixed in 2% wt/vol paraformaldehyde in PBS for 10 min at room temperature. The fixative was removed with HBSS (800g, 10 min) and HBSS (0.5 ml) was added to each well before imaging.

LPS inhibition assay. SNAPP S16 (50 μ l) was incubated with LPS from *E. coli* O111:B4 (50 μ l) in MEM in a 96-well plate at 37 °C for 1 h. *E. coli* cells (which gave an optical density reading of ~ 0.7 at 650 nm) were diluted to 2.5×10^6 cells ml $^{-1}$ in MEM and 100 μ l of the bacteria solution was added to the S16-LPS mixture. The final concentration of S16 was kept at 4 μ g ml $^{-1}$, whereas the LPS concentration was varied from 2 to 1,000 μ g ml $^{-1}$. The 96-well plate was then incubated at 37 °C for 90 min. A 50 μ l aliquot was taken from each well, transferred to a second 96-well plate, and 100 μ l of saline and dye mixture (that is, saline with 0.1% SYTO 9 and 0.1% PI) was added. Each well in the second 96-well plate was analysed with a Cell Lab Quanta SC MPL flow cytometer (Beckman Coulter) to determine the percent of PI-positive cells. Two independent runs of the assay were conducted and two replicates were used in each run for each variation.

Kinetics of antimicrobial activity. SNAPP S16 (at a final concentration of 8 μ g ml $^{-1}$) was incubated with *E. coli* cells (at a final concentration of 1.25×10^6 cells ml $^{-1}$) in MEM at 37 °C. Aliquots were taken at $t = 0, 15, 30$ and 90 min for analysis to determine the c.f.u. ml $^{-1}$ (see procedure for the measurement of MBC) and percent of PI-positive cells (via flow cytometry using a Cell Lab Quanta SC MPL flow cytometer (Beckman Coulter)). An untreated control group was also included. Two independent assay experiments were conducted and two replicates were used in each experiment for each variation.

Preparation of large unilamellar vesicles for dye release (pore formation) and lucigenin (chloride ion transport) based assays. To represent a model of an *E. coli* cytoplasmic membrane, large unilamellar vesicles (LUVs) consisting of 1-palmitoyl-2-oleoyl-sn-glycero-3-phosphoethanolamine (POPE) and 1-palmitoyl-2-oleoyl-sn-glycero-3-phosphoglycerol (POPG) at a 7:3 mole ratio 38 were used to encapsulate 2 mM rhodamine dextran (70 kDa; RD-40) and 2 mM fluorescein dextran (4 kDa; FD-4) in 10 mM Tris and 5 mM NaCl buffer solution (pH 7.3) for the dye release assay or 2 mM lucigenin solution containing NaCl (100 mM) and sodium phosphate salt (10 mM, pH 7.3) for the chloride ion transport assay, using the LUV preparation method we have previously described 50 . The dye release assay was performed as previously described 50 and the chloride ion transport assay conducted as described by Elie and co-authors 39 . LUVs were incubated (0.5 h for the dye release experiment or overnight for the chloride ion transport assay) with SNAPP S16 or control AMP maculatin 1.1 at lipid-to-peptide molar ratios ranging from 50:1 to 10,000:1. To afford complete dye release or chloride ion transport, control LUVs were treated with 0.5% vol/vol Triton X-100. All measurements were made with a Varian Cary Eclipse spectrophotometer using a 4 mm path-length quartz microfluorimeter cell (Starna) for the dye release experiment or a FLUOstar Optima

plate reader (BMG Labtech) for the chloride ion transport assay. Dye release or chloride ion transport was presented as the percent of fluorescence of RD-70 and FD-4 or lucigenin, respectively, compared to the Triton X-100 control. Data are representative of two independent assays completed in duplicate.

Membrane potential assay. Membrane potential was determined by flow cytometry using a BacLight Bacterial Membrane Potential Kit (Invitrogen). When at low concentrations, the dye DiOC₂(3) exhibits green fluorescence in all bacterial cells. The fluorescence shifts towards red emission as the dye molecules become more concentrated and self-associate in healthy cells that are maintaining a membrane potential. *E. coli* cells were inoculated to mid-log phase. Viable cells were then diluted to 2.5×10^6 cells ml⁻¹ in PBS and added with different concentrations (0.5x, 1x and 2x MBC) of SNAPP **S16**. A fully depolarized control was provided by the addition to the untreated cells of the proton ionophore carbonyl cyanide 3-chlorophenylhydrazone (CCCP) at a final concentration of 5 mM. Before a 1 h incubation at 37 °C, 30 mM DiOC₂(3) was added to all samples. Membrane potential was determined by a Cell Lab Quanta SC MPL flow cytometer (Beckman Coulter) as the ratio of cells that exhibited red fluorescence (FL-3) to those that displayed green fluorescence (FL-1). Gates were drawn based on the untreated (polarized) and CCCP-treated (fully depolarized) controls. Data are representative of two independent assays completed in duplicate.

RNA extraction and reverse transcriptase polymerase chain reaction (RT-PCR) analysis for programmed cell death pathways. To determine if the star peptide polymers induced PCD, *E. coli* cells were incubated with **S16** at 1x and 5x the MBC, after which the mRNA levels of *recA*, *lexA* and *mazEF* relative to control genes and untreated *E. coli* were determined by RT-PCR^{40,41,51}. *E. coli* ATCC 25922 was grown overnight at 37 °C in LB broth and used to freshly inoculate LB broth (2% vol/vol inoculum), and was grown to mid-log phase ($OD_{600} = 0.6$) at 37 °C. A 200 µl aliquot of the cell suspension was mixed with 1 µl of Syto9 and 1 µl of PI and counted on the Cell Lab Quanta SC MPL flow cytometer (Beckman Coulter). After counting, cells were collected by centrifugation at 8,000g for 10 min at 4 °C, washed twice in MEM and finally resuspended at 2×10^6 cells ml⁻¹ in MEM. A 500 µl aliquot of a stock solution of SNAPP **S16** (final concentration of 1 x MBC or 5 x MBC) was added to 500 µl (final concentration of 1×10^6 cells ml⁻¹) of *E. coli* cells. Following incubation (4 h), bacterial cells were collected by centrifugation at 8,000g for 10 min at 4 °C and immediately resuspended in 1 ml RNAprotect Bacteria Reagent (Qiagen).

Total RNA was extracted using the RNAprotect bacterial reagent and RNEasy kit (Qiagen). Cells were collected by centrifugation at 8,000g for 10 min at 4 °C and resuspended in 100 µl TE buffer (10 mM TrisCl, 1 mM EDTA, pH 8.0) containing 1 mg ml⁻¹ lysozyme. After 5 min incubation at room temperature, 350 µl of buffer RLT was added and the solution mixed by vortexing. Ethanol (250 µl) was then added and the entire 700 µl was added onto an RNEasy spin column and centrifuged at 16,000g for 1 min. The membrane was washed with 700 µl of buffer RW1 followed by 500 µl of RPE buffer. A final centrifugation at 16,000g for 1 min was performed to dry the membrane. RNase free water (50 µl) was added to the membrane and the RNA was eluted by centrifugation at 16,000g for 1 min. RNA was quantified by absorbance (260 nm/280 nm) using a Nanodrop spectrophotometer (Thermo Scientific).

Extracted RNA was immediately DNase-treated using the TURBO DNA-free kit (Ambion). Briefly, 5 µg of RNA was combined with 2 µl of 10x DNase buffer, 1 µl of DNase and sufficient water to make up a 20 µl reaction volume. The reaction was incubated for 20 min at 37 °C, after which a further 1 µl of DNase was added and the reaction was incubated for another 20 min at 37 °C. Following this second incubation, 2 µl of DNase inactivation reagent was added. After 5 min incubation at room temperature with occasional mixing, the inactivation reagent was pelleted by centrifugation at 10,000g for 1 min and the supernatant collected.

Reverse transcription was performed using the iScript Reverse Transcription Supermix (Bio-Rad). Briefly, 1 µg (4 µl) of the DNase-treated RNA extract was combined with 4 µl of iScript master mix and 12 µl of RNase free water. The reverse transcription reaction was performed with a 5 min, 25 °C priming step, a 30 min, 42 °C extension step, and a 5 min, 85 °C inactivation step. A no-reverse transcription reaction was also set up using 1 µg (4 µl) of the DNase-treated RNA extraction combined with 16 µl of RNase free water.

RT-PCR was performed using iTaq Universal SYBR Green Supermix (Bio-Rad). Template cDNA (25 ng, 1 µl) was combined with 0.8 µl of forward primer (5 nM), 0.8 µl of reverse primer (5 nM) and 10 µl of SYBR Green Supermix. Primers used for the RT-PCR; *recA* (*For*) AGATCCTCTACGGCGAAGGT, (*rev*) CCTGCTTCTCGATCAGCTT; *lexA* (*For*) GACTTGCTGGCAGTCATAA, (*rev*) TCAGGGCTTAACGGTAACCT; *MazEF-1* (*For*) CTTCTGCTCCCTCTTG, (*rev*) CGTTGGGGAAATTCAACCG; 16S rRNA (*For*) TGTAGCGGTGAAATGCGTAGA, (*rev*) CACCTGAGCGTCAGTCTTCGT⁵¹. Thermal cycling was performed by 40 cycles of 95 °C for 15 s, 60 °C for 15 s and 72 °C for 15 s. A positive control of genomic DNA and a no-reverse transcription control were included in each cycling run. Cycling was performed on a Rotor Gene RG-3000A Thermal Cycler running Rotor-Gene V6.1 software (Corbett Research). Analysis of the PCR was performed using LinRegPCR software version 2015.3. Comparative cycle threshold (Ct) analysis was performed according to the method of Schmittgen and Livak⁵².

ROS production. *E. coli* cells (which gave an OD reading of ~0.7 at 650 nm) were diluted to 2.5×10^6 cells ml⁻¹ in MEM and 100 µl of the bacteria solution was added to each well containing either MEM (untreated control) or the test compound(s) at the desired concentrations (100 µl). The 96-well plate was then incubated at 37 °C for 90 min. The cells were then stained with the CellROX Orange Reagent at a final concentration of 750 nM following the manufacturer's instructions and were incubated for 1 h at 37 °C. The cells were analysed on the Cell Lab Quanta SC MPL flow cytometer (Beckman Coulter) and the fluorescence from the CellROX Orange Reagent was measured on FL-3. A minimum of two independent experiments were conducted for the assay, and two technical replicates were used in each experiment. Data are expressed as mean ± s.d.

Effect of ALD inhibition on the membrane disruption ability of SNAPP S16. *E. coli* cells (which gave an optical density reading of ~0.7 at 650 nm) were diluted to 2.5×10^6 cells ml⁻¹ in MHB, and 5 ml of the bacterial cell solution was added to an equivolume of doxycycline hydrate (to yield a final concentration equivalent to its MIC of 0.5 µg ml⁻¹). The mixture was incubated at 37 °C for 4 h and the cells were recovered via centrifugation (3,000g, 10 min) at the end of the incubation period. The recovered cells (100 µl per well) were then incubated at 37 °C for a further 90 min in the absence or presence of SNAPP (at 0.5x and 1 x MBC, 100 µl per well) in a 96-well plate. A 50 µl aliquot was taken from each well, transferred to a second 96-well plate, and 100 µl of saline and dye mixture (that is, saline with 0.1% of SYTO 9 and 0.1% of PI) was added. Each well in the second 96-well plate was analysed with a Cell Lab Quanta SC MPL flow cytometer (Beckman Coulter) to determine the percent of PI-positive cells. Two independent runs of the assay were conducted and two replicates were used in each run for each variation.

Cryo-TEM. Star peptide polymer **S16** (35 µg ml⁻¹ in MHB; 15 and 35 µg ml⁻¹ in MEM), melittin (64 µg ml⁻¹ in MHB) or ovispirin (19 µg ml⁻¹ in MHB) was incubated with *E. coli* cells (1.25×10^6 cells ml⁻¹ in MHB or MEM, prepared as described in the measurement of MBC) at 37 °C for 90 min. After incubation, the cells were pelleted (10,000g, 20 min), washed with pre-filtered PBS and resuspended in the same buffer (~10–30 µl). Subsequent steps were taken based on the protocol previously described⁵³.

Statistical analysis. The data obtained were determined to be normally distributed. Homogeneity of variances was assessed using Levene's test (SPSS for Windows, version 12). Statistical analysis was also performed using a one-way classification of ANOVA and Student's *t*-test (two-tailed), where differences were regarded as statistically significant with probability $P < 0.05$.

Received 18 February 2016; accepted 2 August 2016;
published 12 September 2016

References

- World Health Organization. *Antimicrobial Resistance: Global Report on Surveillance 2014* (WHO, 2014).
- Rice, L. B. Federal funding for the study of antimicrobial resistance in nosocomial pathogens: no ESKAPE. *J. Infect. Dis.* **197**, 1079–1081 (2008).
- Rice, L. B. Progress and challenges in implementing the research on ESKAPE pathogens. *Infect. Control Hosp. Epidemiol.* **31**, S7–S10 (2010).
- Taubes, G. The bacteria fight back. *Science* **321**, 356–361 (2008).
- Xu, Z., Flavin, M. T. & Flavin, J. Combating multidrug-resistant Gram-negative bacterial infections. *Exp. Opin. Invest. Drugs* **23**, 163–182 (2014).
- Lee, J. H., Jeong, S. H., Cha, S. & Lee, S. H. A lack of drugs for antibiotic-resistant Gram-negative bacteria. *Nat. Rev. Drug Discov.* **6**, 29–40 (2007). doi:10.1038/nrd2201-c1.
- Le Moual, H. & Gruenheid, S. Resistance to antimicrobial peptides in Gram-negative bacteria. *FEMS Microbiol. Lett.* **330**, 81–89 (2012).
- Brogden, K. A. Antimicrobial peptides: pore formers or metabolic inhibitors in bacteria? *Nat. Rev. Microbiol.* **3**, 238–250 (2005).
- Kohanski, M. A., Dwyer, D. J. & Collins, J. J. How antibiotics kill bacteria: from targets to networks. *Nat. Rev. Microbiol.* **8**, 423–435 (2010).
- Zasloff, M. Antimicrobial peptides of multicellular organisms. *Nature* **415**, 389–395 (2002).
- Melo, M. N., Dugourd, D. & Castanho, M. A. Omiganan pentahydrochloride in the front line of clinical applications of antimicrobial peptides. *Recent Pat. Antiinfect. Drug Discov.* **1**, 201–207 (2006).
- Hancock, R. E. W. & Sahl, H. Antimicrobial and host-defense peptides as new anti-infective therapeutic strategies. *Nat. Biotechnol.* **24**, 1551–1557 (2006).
- Zhou, C. et al. High potency and broad-spectrum antimicrobial peptides synthesized via ring-opening polymerization of α -amino acid-N-carboxyanhydrides. *Biomacromolecules* **11**, 60–67 (2010).
- Engler, A. C. et al. Effects of side group functionality and molecular weight on the activity of synthetic antimicrobial polypeptides. *Biomacromolecules* **12**, 1666–1674 (2011).
- Sulistio, A., Blencowe, A., Widjaya, A., Zhang, X. & Qiao, G. G. Development of functional amino acid-based star polymers. *Polym. Chem.* **3**, 224–234 (2012).

16. Sulistio, A., Widjaya, A., Blencowe, A., Zhang, X. & Qiao, G. G. Star polymers composed entirely of amino acid building blocks: a route towards stereospecific, biodegradable and hierarchically functionalized stars. *Chem. Commun.* **47**, 1151–1153 (2011).
17. Wu, W., Wang, W. & Li, J. Star polymers: advances in biomedical applications. *Prog. Polym. Sci.* **46**, 55–85 (2015).
18. Lam, S. J. *et al.* Peptide-based star polymers as potential siRNA carriers. *Aust. J. Chem.* **67**, 592–597 (2014).
19. Byrne, M. *et al.* Molecular weight and architectural dependence of well-defined star-shaped poly(lysine) as a gene delivery vector. *Biomater. Sci.* **1**, 1223–1234 (2013).
20. Sulistio, A. *et al.* Folic acid conjugated amino acid-based star polymers for active targeting of cancer cells. *Biomacromolecules* **12**, 3469–3477 (2011).
21. Nederberg, F. *et al.* Biodegradable nanostructures with selective lysis of microbial membranes. *Nat. Chem.* **3**, 409–414 (2011).
22. Liu, L. *et al.* Self-assembled cationic peptide nanoparticles as an efficient antimicrobial agent. *Nat. Nanotech.* **4**, 457–463 (2009).
23. Ng, V. W. L., Ke, X., Lee, A. L. Z., Hedrick, J. L. & Yang, Y.-Y. Synergistic co-delivery of membrane-disrupting polymers with commercial antibiotics against highly opportunistic bacteria. *Adv. Mater.* **25**, 6730–6736 (2013).
24. Campos, M. A. *et al.* Capsule polysaccharide mediates bacterial resistance to antimicrobial peptides. *Infect. Immun.* **72**, 7107–7114 (2004).
25. Llobet, E., Tomas, J. M. & Bengoechea, J. A. Capsule polysaccharide is a bacterial decoy for antimicrobial peptides. *Microbiology* **154**, 3877–3886 (2008).
26. Melo, M. N., Ferre, R. & Castanho, M. A. R. B. Antimicrobial peptides: linking partition, activity and high membrane-bound concentrations. *Nat. Rev. Microbiol.* **7**, 245–250 (2009).
27. Choi, H., Chakraborty, S., Liu, R., Gellman, S. H. & Weisshaar, J. C. Medium effects on minimum inhibitory concentrations of nylon-3 polymers against *E. coli*. *PLoS ONE* **9**, e104500 (2014).
28. Davis, S. D. Activity of gentamicin, tobramycin, polymyxin B, and colistimethate in mouse protection tests with *Pseudomonas aeruginosa*. *Antimicrob. Agents Chemother.* **8**, 50–53 (1975).
29. Velkov, T. *et al.* Teaching ‘old’ polymyxins new tricks: new-generation lipopeptides targeting Gram-negative ‘superbugs’. *ACS Chem. Biol.* **9**, 1172–1177 (2014).
30. Li, W. *et al.* Proline-rich antimicrobial peptides: potential therapeutics against antibiotic-resistant bacteria. *Amino Acids* **46**, 2287–2294 (2014).
31. Hilchie, A. L., Wuerth, K. & Hancock, R. E. W. Immune modulation by multifaceted cationic host defense (antimicrobial) peptides. *Nat. Chem. Biol.* **9**, 761–768 (2013).
32. Lee, H. J. *et al.* Synergistic activity of colistin and rifampin combination against multidrug-resistant *Acinetobacter baumannii* in an *in vitro* pharmacokinetic/pharmacodynamic model. *Antimicrob. Agents Chemother.* **57**, 3738–3745 (2013).
33. Benincasa, M., Pacor, S., Gennaro, R. & Scocchi, M. Rapid and reliable detection of antimicrobial peptide penetration into Gram-negative bacteria based on fluorescence quenching. *Antimicrob. Agents Chemother.* **53**, 3501–3504 (2009).
34. Alves, C. S. *et al.* *Escherichia coli* cell surface perturbation and disruption induced by antimicrobial peptides BP100 and pepR. *J. Biol. Chem.* **285**, 27536–27544 (2010).
35. Li, W. *et al.* Multimerization of a proline-rich antimicrobial peptide, CheX-Arg20, alters its mechanism of interaction with the *Escherichia coli* membrane. *Chem. Biol.* **22**, 1250–1258 (2015).
36. Fjell, C. D., Hiss, J. A., Hancock, R. E. W. & Schneider, G. Designing antimicrobial peptides: form follows function. *Nat. Rev. Drug Discov.* **11**, 37–51 (2012).
37. Freire, J. M. *et al.* Monitoring antibacterial permeabilization in real time using time-resolved flow cytometry. *Biochim. Biophys. Acta* **1848**, 554–560 (2015).
38. Morein, S., Andersson, A., Rilfors, L. & Lindblom, G. Wild-type *Escherichia coli* cell regulate the membrane lipid composition in a ‘window’ between gel and non-lamellar structures. *J. Biol. Chem.* **271**, 6801–6809 (1996).
39. Elie, C. R., Hebert, A., Charbonneau, M., Haiun, A. & Schmitzer, A. R. Benzimidazolium-based synthetic chloride and calcium transporters in bacterial membranes. *Org. Biomol. Chem.* **11**, 923–928 (2013).
40. Erental, A., Sharon, I. & Engelberg-Kulka, H. Two programmed cell death systems in *Escherichia coli*: apoptotic-like death is inhibited by the mazEF-mediated death pathway. *PLoS Biol.* **10**, e1001281 (2012).
41. Bayles, K. W. Bacterial programmed cell death: making sense of a paradox. *Nat. Rev. Microbiol.* **12**, 63–69 (2014).
42. Erental, A., Kalderon, Z., Saada, A., Smith, Y. & Engelberg-Kulka, H. Apoptosis-like death, an extreme SOS response in *Escherichia coli*. *mBio* **5**, e01426–14 (2014).
43. Henriques, S. T., Melo, M. N. & Castanho, M. A. R. B. Cell-penetrating peptides and antimicrobial peptides: how different are they? *Biochem. J.* **399**, 1–7 (2006).
44. Henriques, S. T., Melo, M. N. & Castanho, M. A. R. B. How to address CPP and AMP translocation? Methods to detect and quantify peptide internalization *in vitro* and *in vivo*. *Mol. Membr. Biol.* **24**, 173–184 (2007).
45. Hancock, R. E. W. & Chapple, D. S. Peptide antibiotics. *Antimicrob. Agents Chemother.* **43**, 1317–1323 (1999).
46. Sato, H. & Feix, J. B. Peptide-membrane interactions and mechanisms of membrane destruction by amphipathic α -helical antimicrobial peptides. *Biochim. Biophys. Acta Biomembranes* **1758**, 1245–1256 (2006).
47. Morones-Ramirez, J. R., Winkler, J. A., Spina, C. S. & Collins, J. J. Silver enhances antibiotic activity against Gram-negative bacteria. *Sci. Transl. Med.* **5**, 190ra81 (2013).
48. Gullberg, E. *et al.* Selection of resistant bacteria at very low antibiotic concentrations. *PLoS Pathogens* **7**, e1002158 (2011).
49. Siegel, R. E. Emerging Gram-negative antibiotic resistance: daunting challenges declining sensitivities, and dire consequences. *Respir. Care* **53**, 471–479 (2008).
50. Sani, M.-A. *et al.* Maculatin 1.1 disrupts *Staphylococcus aureus* lipid membranes via a pore mechanism. *Antimicrob. Agents Chemother.* **57**, 3593–3600 (2013).
51. Moritz, E. M. & Hergenrother, P. J. Toxin-antitoxin systems are ubiquitous and plasmid-encoded in vancomycin-resistant enterococci. *Proc. Natl. Acad. Sci. USA* **104**, 311–316 (2007).
52. Livak, K. J. & Schmittgen, T. D. Analysis of relative gene expression data using real-time quantitative PCR and the $2^{-\Delta\Delta C(T)}$ method. *Methods* **25**, 402–408 (2001).
53. Chen, Y.-Y. *et al.* The outer membrane protein LptO is essential for O-deacylation of LPS and the co-ordinated secretion and attachment of A-LPS and CTD proteins in *Porphyromonas gingivalis*. *Mol. Microbiol.* **79**, 1380–1401 (2011).

Acknowledgements

G.G.Q. acknowledges financial support from the Australian Research Council under the Future Fellowship (FT110100411) scheme. E.C.R. acknowledges financial support from the Australian Government, Department of Industry, Innovation and Science. S.J.L. acknowledges the Australian Government for providing an International Postgraduate Research Scholarship (IPRS) and an Australian Postgraduate Award (APAInt). The authors thank the Advanced Fluorescence Imaging Platform at the Materials Characterisation and Fabrication Platform (The University of Melbourne) for instrument access. The authors thank B. Hibbs for assistance with the Delta Vision OMX V4 BLAZE, S. Lowe for technical laboratory assistance and J. Li for the CMDR bacterial strains.

Author contributions

G.G.Q., N.M.O.B.-S., A.B. and E.C.R. oversaw the project. S.J.L. synthesized and characterized the polymers, performed the *in vitro* and imaging experiments and wrote the paper, with intellectual input from E.H.H.W., A.S. and A.B. N.P. contributed to the *in vitro* experiments. J.C.L. contributed to the *in vivo* animal models and immune cell phenotyping and *in vitro* experiments. J.A.H. contributed to the RT-PCR and *in vitro* experiments. Y.-Y.C. contributed to the cryo-TEM experiments. All authors gave suggestions to improve the presentation of the paper.

Additional information

Supplementary information is available for this paper. Reprints and permissions information is available at www.nature.com/reprints. Correspondence and requests for materials should be addressed to E.C.R. and G.G.Q.

Competing interests

The authors declare no competing financial interests.